https://doi.org/10.5194/essd-2026-639
Preprint. Discussion started: 29 September 2026

Open Access Earth System Science Data Discussions

The satellite-only gravity field model GOCO2025s

Felix Öhlinger[1], Torsten Mayer-Gürr[1], Sandro Krauss[1], Patrick Dumitraschkewitz[1], Andreas Strasser[1], Barbara Süsser-Rechberger[2], Jan Martin Brockmann[3,4], and Josef Niedermaier[5]

[1]Institute of Geodesy, Graz University of Technology, Steyrergasse 30/III, 8010 Graz, Austria
[2]Institute of Physics, University of Graz, Universitätsplatz 5, 8010 Graz, Austria
[3]Institute of Geodesy and Geoinformation, University of Bonn, Nußallee 17, 53115 Bonn, Germany
[4]High Performance Computing and Analytics Lab, University of Bonn, Nußallee 17, 53115 Bonn, Germany
[5]Institute for Astronomical and Physical Geodesy, Technical University of Munich, Arcistraße 21, 80333 Munich, Germany

Correspondence: Felix Öhlinger (felix.oehlinger@tugraz.at)

Abstract. GOCO2025s is a global gravity field model represented by spherical harmonic coefficients up to degree and order 300, with constrained secular, annual, and semi-annual variations up to degree and order 200. It is derived from 23 years of satellite data, incorporating observations from the dedicated gravity field missions Gravity field and steady-state Ocean Circulation Explorer (GOCE), Gravity Recovery and Climate Experiment (GRACE), and GRACE Follow-On (GRACE-FO), as well as kinematic orbits of 18 low Earth orbit satellites and satellite laser ranging observations to 9 passive geodetic satellites. The complementary measurement principles of the different satellite missions and their strengths in determining specific parts of the spherical harmonic spectrum were exploited by combining the data at the normal equation level, with emphasis on the stochastic modeling of each contribution. Particular focus was placed on the inclusion of GRACE-FO laser ranging interferometer (LRI) data, which provided the dominant contribution to the estimation of the spherical harmonic coefficients between degrees 70 and 200. All processing steps, except for the determination of the GOCE normal equations, were carried out at the Institute of Geodesy at Graz University of Technology (TUG) employing up-to-date background models. The consistent in-house processing of nearly all satellite data, using the Gravity Recovery Object Oriented Programming System (GROOPS) software package, minimized errors arising from inconsistencies of different algorithms or models being applied.

The individual files of the GOCO2025s model (Öhlinger et al., 2025) are available at the TUG repository and identified with the following DOI: 10.3217/f48p8-8h651. They comprise the static and time-dependent gravity field coefficients and their respective uncertainty information, all parts of the normal equation system of the static gravity field, and the gravitational potential of non-tidal atmospheric and ocean masses already included in GOCO2025s.

1 Introduction

The Earth's gravity field reflects the spatial distribution of mass across the planet, making it a key observable for investigating the dynamics of the Earth system. Models of the static gravity field describe the long-term, time-averaged shape of the Earth, which is essential for a wide range of geoscientific applications, including oceanography, continental hydrology, sea level and ice mass changes (Tapley et al., 2019), as well as geoid determination (Barthelmes, 2013) and height system realization (Rummel, 2012). Global gravity field models are also a prerequisite for simulation studies of next-generation satellite missions

https://doi.org/10.5194/essd-2026-639
Preprint. Discussion started: 29 September 2026

(Pail et al., 2019). Here, highly accurate background models form the basis for end-to-end mission simulators. Such studies have been conducted, among others, for GRACE-Continuity and the Next Generation Gravity Mission (Daras et al., 2024).

Gravity field models based entirely on satellite observations benefit from a consistent data accuracy and provide a globally homogeneous quality. In contrast, models which additionally include terrestrial, shipborne or altimetry-derived gravity data achieve higher spatial resolution at the cost of regionally varying model quality due to the heterogeneous distribution and accuracy of the gravity observations. The globally consistent measurement accuracy of satellite observations also allows for adequate stochastic modeling at the observation level (Ellmer, 2018). Together with the incorporation of background model uncertainties (Kvas and Mayer-Gürr, 2019), this results in realistic formal errors for the derived gravity field solutions.

Dedicated gravity field satellite missions such as the CHAllenging Minisatellite Payload (CHAMP, Reigber et al., 1999), the Gravity Recovery and Climate Experiment (GRACE, Tapley et al., 2004, 2019) and the Gravity field and steady-state Ocean Circulation Explorer (GOCE, Floberghagen et al., 2011) observe changes of the gravity field using different measurement techniques. While CHAMP made use of its GPS receiver to recover the Earth's gravity field, GOCE was additionally equipped with a gradiometer to measure the second derivative of the gravitational potential. The two GRACE satellites used a K/Ka-band ranging (KBR) instrument to determine the distance changes between each other and consequently derive gravity changes. GRACE Follow-On (GRACE-FO, Landerer et al., 2020) – the successor mission of GRACE – additionally carries a laser ranging interferometer (LRI) alongside the KBR instrument. The distinct measurement techniques and altitudes of the spacecraft imply that different parts of the spectrum of the gravity signal can be determined by the respective mission. While GRACE and GRACE-FO, using low-low satellite-to-satellite tracking (SST) at an altitude of about 500 km, are primarily sensitive to the medium and long wavelengths, GOCE, using gradiometry at 250 km altitude, is particularly sensitive to the short wavelengths, enabling a much higher spatial resolution. However, GOCE cannot be used to estimate the time-variable part of the gravity field due to the spectral noise characteristics of the gravity gradient observations, whereas GRACE-like missions are designed to observe these temporal variations. Apart from dedicated gravity field missions, satellite observations from other missions can also contribute to gravity field estimation. In particular, kinematic orbit positions of low Earth orbit (LEO) satellites, derived from onboard GPS observations, provide information on the long and medium wavelengths. Additionally, satellite laser ranging (SLR) observations to high-flying geodetic satellites can be used to determine the very long-wavelength part of the gravity signal. Combined gravity field models are designed to benefit from these complementary observation types and to compensate for deficiencies of the individual contributions. Several such models exist, including Tongji-GMMG2021S (Chen et al., 2018, 2022), WHU-SWPU-GOGR2022S (Zhao et al., 2023) or the models of the GOCO series (Pail et al., 2010; Goiginger et al., 2011; Mayer-Gürr et al., 2012, 2015; Kvas et al., 2021), which typically combine GRACE and GOCE data.

The primary motivation for the new GOCO release – GOCO2025s – was the incorporation of the GRACE-FO data set and, in particular, the analysis of the contribution of the LRI observations. Originally designed as a technology demonstrator for future GRACE-like satellite missions, the LRI has proven its capability of capturing gravity signals which are one order of magnitude smaller compared to the sensitivity of the KBR system (Ghobadi-Far et al., 2020). This study investigates the impact of these observations and the improvements introduced in the new GOCO release as part of a reprocessing campaign for GRACE, GRACE-FO, kinematic orbit, and SLR data. Consistent up-to-date background models were applied, including

https://doi.org/10.5194/essd-2026-639
Preprint. Discussion started: 29 September 2026

a newly developed ocean tide model and a refined autoregressive (AR) model to account for background model uncertainties associated with global atmosphere and ocean mass variability and hydrology. The determination of GOCO2025s also served to assess the benefit of consistently processing almost all satellite data in-house with the same software. In particular, the recently developed SLR functionality allowed the normal point data to be included as an internally computed contribution. With the exception of the GOCE normal equations, all computations were carried out at the Institute of Geodesy at Graz University of Technology (TUG) using the Gravity Recovery Object Oriented Programming System (GROOPS, Mayer-Gürr et al., 2021) software toolkit.

In this paper, the satellite-only gravity field model GOCO2025s is presented. Section 2 gives information about the employed satellite data, the parameterization of the respective normal equations, and the background models. The stochastic modeling of the individual contributions is outlined in Sect. 3, and the combination process is discussed in Sect. 4. In Sect. 5, GOCO2025s is validated against independent data sets, comprising GNSS, leveling, and altimetry, and compared with other global gravity field models.

2 Data acquisition - Satellite data contributions and background models

The GOCO2025s gravity field model comprises satellite data from GOCE, GRACE, and GRACE-FO, as well as kinematic orbits from 18 LEO satellites, and SLR observations to 9 passive geodetic satellites. Information about the observations of the individual satellite contributions is summarized in Table 1, and the background models used for all the processing, except for the GOCE normal equations, are listed in Table 2.

Table 1. Satellite data used for GOCO2025s: The time period refers to the data employed in the combination process and does not have to coincide with the first or last data available for any of the satellite missions. December 2024 was defined as the last month of the considered time span for GOCO2025s. Specifically for GRACE and GRACE-FO, some monthly solutions were not considered due to missing data or deteriorated quality. The period set for the kinematic orbits of LEO satellites starts with the first solution determined for CHAMP. All LEO orbits were estimated for the entire respective mission duration.

Satellite data	No. of satellites	Period (inclusive)	Principle observation type	Source
GOCE	1	2009-10 – 2013-10	Gradiometry	ESA
GRACE	2	2002-04 – 2016-08	KBR, kinematic orbits	JPL, TUG
GRACE-FO	2	2018-06 – 2024-12	KBR, LRI, kinematic orbits	JPL, AEI, TUG
LEO satellites	18	2002-01 – 2024-12	Kinematic orbits[a]	TUG
SLR	9	2006-01 – 2024-12	Normal points	ILRS

[a] Kinematic orbit products produced by TUG are available at: https://www.tugraz.at/institute/ifg/downloads/satellite-orbit-products

https://doi.org/10.5194/essd-2026-639
Preprint. Discussion started: 29 September 2026

2.1 Gravity field and steady-state Ocean Circulation Explorer (GOCE)

The GOCE contribution to GOCO2025s is derived from the satellite gravity gradiometry (SGG) normal equations generated within the processing of the GO_CONS_EGM_TIM_RL06 solution (Brockmann et al., 2019, 2021). These normal equations were determined using the time-wise approach (Pail et al., 2011) and are based solely on calibrated SGG observations from the entire operational period of the mission. They are therefore independent of any other gravity field information and well-suited for the combination with other satellite data sets. The rigorous stochastic modeling of the SGG observations provides realistic accuracy information of the model coefficients, which is essential for a consistent combination of GOCO2025s at normal equation level.

The official GO_CONS_EGM_TIM_RL06 solution is based on SGG observations, as well as on GOCE kinematic orbits, and a regularization strategy to account for the polar gap and improve the signal-to-noise ratio in the high-degree coefficients (Brockmann et al., 2021). For GOCO2025s, however, only the unconstrained SGG normal equations parameterized in terms of spherical harmonics from degree 2 to 300 were used to determine the static part of the gravity field. Polar gap regularization was not required for GOCO2025s due to the combination with other satellite data, and the regularization for the high-degree coefficients is described in Sect. 4. The normal equations of the GOCE kinematic orbit solution were determined independently, as described in Sect. 2.4.

2.2 Gravity Recovery and Climate Experiment (GRACE)

Monthly gravity field solutions from the entire operational period of GRACE were reprocessed for GOCO2025s following the processing strategy outlined in Kvas et al. (2019), using the background models listed in Table 2. The normal equations were set up employing the variational equation approach (Ellmer, 2018), parameterizing the static part of the gravity field up to degree and order 230 and the long-term temporal gravity variations, represented by a trend, an annual, and a semi-annual oscillation, up to degree and order 150. The official GRACE L1B RL03 observation data published by the Jet Propulsion Laboratory (JPL, 2018), together with the in-house processed kinematic GRACE orbits (see Sect. 2.4), were used. Emphasis was placed on a realistic uncertainty description of the monthly solutions. The stochastic modeling of the observations and the background model uncertainties is described in detail by Ellmer (2018) and Kvas and Mayer-Gürr (2019), and summarized in Sect. 3.2 and Sect. 3.3, respectively. Due to missing or degraded observation data, mainly related to the outage of the accelerometer on GRACE-B, the gravity field solutions from September 2016 to June 2017 were excluded from the combination. The remaining monthly normal equations were accumulated and subsequently used to estimate the static part and the long-term temporal variations of GOCO2025s.

2.3 Gravity Recovery and Climate Experiment Follow-On (GRACE-FO)

For GRACE-FO, monthly solutions from June 2018 to December 2024 were reprocessed using the background models from Table 2, employing a processing approach similar to the one used for GRACE. However, both types of SST observations, KBR and LRI, were used whenever the two data sets were available. In nominal fine-pointing mode, both SST observation

https://doi.org/10.5194/essd-2026-639
Preprint. Discussion started: 29 September 2026

types were processed. To reduce thruster activation and overall fuel consumption, GRACE-FO has been operated in a relaxed pointing mode since July 2023 (similar to the mode used in January and February 2023). This mode allows for greater pointing offsets, yet the LRI is not collecting nominal science data anymore, and only KBR ranging observations are available (Landerer et al., 2023). The official GRACE-FO L1B RL04 data released by JPL (2019) were used to derive the monthly gravity field solutions. However, for the LRI measurements, the LRI1B v54 data set from Müller et al. (2024), processed at the Max-Planck Institute for Gravitational Physics (Albert Einstein Institute; AEI), was employed. The synthetic accelerometer observations required for the GRACE-D satellite, also known as the accelerometer transplant, were determined in-house using an adjusted version of the approach from Behzadpour et al. (2021). Stochastic modeling for the KBR-only and the dual-SST solutions was performed as outlined in Sect. 3.2. The parametrization of the static and temporal parts of the gravity field for the KBR-only solutions was the same as for GRACE. For the dual-SST solutions, however, the static gravity field was estimated up to degree and order 250.

2.4 Kinematic orbits of low Earth orbit (LEO) satellites

Kinematic orbits of 18 LEO satellites were estimated for GOCO2025s following the precise orbit determination (POD) approach from Süsser-Rechberger et al. (2022), which is based on raw GPS phase and code observations on all available frequencies for daily arcs. Besides GRACE and GRACE-FO, whose kinematic orbits are already included in the corresponding normal equations, kinematic orbit positions were determined for CHAMP, GOCE, Swarm A/B/C, Sentinel-1A/1B/2A/2B/3A/3B/6A, TerraSAR-X and TanDEM-X. The respective normal equations for gravity field recovery were set up monthly using the short-arc integral approach (Mayer-Gürr, 2006). The static part and the temporal variations of the gravity field were parameterized up to degree and order 120 for all satellites except GOCE. The normal equations for GOCE were set up to degree and order 150 due to its lower orbital altitude. The stochastic modeling of the POD-derived kinematic orbit observations in the gravity field estimation process is outlined in Sect. 3.2. Accuracy information in the form of a 3×3 epoch-wise covariance matrix, derived for each satellite during the POD process, was hereby used as a priori information for the stochastic model. Relative weights for all monthly normal equations were estimated using variance component estimation (VCE, Koch and Kusche, 2002). The weighted normal equations were then accumulated over the entire time span of the respective satellite mission, up to December 2024 at the latest.

2.5 Satellite Laser Ranging (SLR)

SLR normal point observations provided by the International Laser Ranging Service (ILRS) to 9 passive geodetic satellites over the period from January 2006 to December 2024 were used in the GOCO2025s combination. For the SLR gravity field recovery, each month was divided into four arcs: the first three arcs cover 7 days each, while the fourth arc consists of the remaining days of the respective month. Compared to the daily arcs used for POD and GRACE/GRACE-FO processing, longer arc lengths are required here due to the sparse and inhomogeneous distribution of the SLR stations and the limited number of observations. The SLR tracking stations were selected in accordance with the ITRF2020 reference frame (Altamimi et al., 2023). Normal point observations from these stations to the satellites AJISAI, BLITS, LAGEOS-1, LAGEOS-2, LARES,

https://doi.org/10.5194/essd-2026-639
Preprint. Discussion started: 29 September 2026

LARES-2, LARETS, Starlette, and Stella were processed, following the approach described in Süsser-Rechberger et al. (2026). Normal equations were set up in weekly batches to degree and order 50 for the static part and the temporal variations of the gravity field. Additional empirical parameters were co-estimated, including a constant acceleration bias for along and cross-track, and a once-per-revolution empirical acceleration for along-track, both parameterized once per day, as well as station range biases, set up once per week for all satellites. In addition, weights for the individual observations and an adjustment factor for each station were determined from the residuals using VCE (see Sect. 3.4). The resulting time series of weekly normal equations was then used to set up a combined normal equation system for both the static gravity field and the temporal variations.

2.6 Background models

Table 2. Background models used for the processing of GRACE, GRACE-FO, the kinematic orbits of 18 LEO satellites, and SLR.

Force / effect	Model	Reference
Earth's gravity field	GOCO06s	Kvas et al. (2021)
– Static, trend, and annual components		
– Co-seismic earthquake signals		
Non-tidal atmosphere and ocean variations	AOD1B RL07	Shihora et al. (2022)
Hydrology	LISFLOOD	Jensen et al. (2025)
Ocean tides	MIXED2025 + GRACE/GRACE-FO corrections	see Sect. 2.6
Atmospheric tides	TiME22	Sulzbach et al. (2022)
Pole tides	IERS2010, linear mean pole	Petit and Luzum (2010)
Ocean pole tides	Desai (2002), linear mean pole	Desai (2002)
Astronomical tides (Moon, sun, planets)	JPL DE432	Folkner (2014)
Solid Earth tides	IERS2010	Petit and Luzum (2010)
Relativistic effects	IERS2010	Petit and Luzum (2010)
Non-conservative forces		
– Solar radiation pressure		Behzadpour (2022)
– Earth radiation pressure	CERES	Wielicki et al. (1996)
– Thermal radiation pressure		Wöske et al. (2019)
– Atmospheric drag	DTM-2020	Bruinsma and Boniface (2021)
	HWM2014	Drob et al. (2015)

When determining a gravity field solution, a functional relationship between the spherical harmonic coefficients and the satellite observations must be established. For the GRACE, GRACE-FO, kinematic orbit, and SLR contribution to GOCO2025s, this functional model is set up by combining dynamically integrated orbits with the observation equations. All background models employed in the precise orbit integration of the respective satellites are listed in Table 2.

https://doi.org/10.5194/essd-2026-639
Preprint. Discussion started: 29 September 2026

GOCO06s (Kvas et al., 2021) was used as the reference gravity field up to degree and order 300 for the static part and up to degree and order 200 for the trend and the annual oscillation. In addition, co-seismic gravity changes, modeled as step functions for three major earthquakes, were taken into account here. The latest release RL07 of the Atmosphere and Ocean De-Aliasing Level-1B (AOD1B) product (Shihora et al., 2022) was employed to account for short-term, non-tidal gravity changes. The corresponding accuracy information, the AOe07 time series of synthetic errors (Shihora et al., 2024), was used for the estimation of the stochastic model of the background model uncertainties, as described in Sect. 3.3. The LISFLOOD hydrological model (De Roo et al., 2000; Knijff et al., 2010; Jensen et al., 2025) was used directly in the gravity field processing for additional dealiasing and also served as input for the stochastic modeling of the background model uncertainties. Since GOCO06s already includes the contributions of the hydrological signal and the non-tidal atmospheric and ocean masses, the static part and the long-term temporal variations of LISFLOOD and AOD1B RL07 were reduced from the models to avoid double consideration. The respective signal components, parameterized in the form of GOCO2025s, are later restored to ensure that GOCO2025s comprises the gravitational potential of the complete Earth.

A new ocean tide model, MIXED2025, was developed in cooperation between TUG, the GFZ Helmholtz Centre for Geosciences, and the Technical University of Munich. The model is available at the website[1] of the Institute of Geodesy at TUG. It is based on GOT5.6 (Ray, 2025) and extended by constituents from FES2022 (Carrere et al., 2022) and TiME22 (Sulzbach et al., 2022). The MIXED2025 model was further supplemented by correction terms, derived from GRACE and GRACE-FO data. For this purpose, zero-constrained corrections for 9 long-period, diurnal and semi-diurnal tidal constituents were estimated up to degree and order 50, together with the static and temporal gravity field, over respective GRACE and GRACE-FO periods.

For satellites, which are not equipped with an accelerometer to measure the non-conservative forces, physical models were used for the simulation of solar radiation pressure, Earth radiation pressure, and thermal radiation pressure, as well as the atmospheric drag acting on the satellites. The Drag Temperature Model 2020 (DTM-2020, Bruinsma and Boniface, 2021) and the Horizontal Wind Model 2014 (HWM2014, Drob et al., 2015) were employed to model the atmospheric density and to account for the force exerted on the satellite surface caused by the remnant atmospheric molecules at the respective satellite altitude. The accelerations caused by solar radiation pressure and Earth radiation pressure were calculated as described in Behzadpour (2022), where monthly mean values for the reflectivity and the emissivity of the Earth's surface were obtained from the Clouds and the Earth's Radiant Energy System (CERES) model (Wielicki et al., 1996). The thermal re-radiation of the satellite was computed according to the algorithm described in Wöske et al. (2019). For the modeling of the non-gravitational forces, macro models of the respective satellites were used, including information about mass, surface areas and their orientation, as well as the physical properties of the material.

[1] https://www.tugraz.at/institute/ifg/downloads/ocean-tides

https://doi.org/10.5194/essd-2026-639
Preprint. Discussion started: 29 September 2026

Open Access Earth System Science Data Discussions

3 Stochastic modeling

When determining a gravity field solution in a least-squares adjustment, an adequate stochastic model is required to properly weight the observations and consequently obtain realistic formal errors. Information about the stochastic characteristics of each satellite contribution used in GOCO2025s is essential for an optimal combination.

3.1 GOCE gravity gradients

Since the gradiometer noise of the individual gravity gradient components is highly temporally correlated, a robustified estimation procedure was employed to model the stochastic characteristics of the noise time series in terms of AR processes (Brockmann et al., 2021). Statistical tests were applied to detect outliers and non-stationary behaviour for each gravity gradient component and continuous data segment before the AR coefficients are estimated and subsequently used for decorrelation. Further details on the processing of GOCE data are provided by Brockmann et al. (2021) and Brockmann (2014).

3.2 GRACE, GRACE-FO and kinematic orbit observations

The stochastic modeling described in this section was employed for gravity field estimation using inter-satellite ranging observations and POD-derived kinematic orbit positions. Consequently, the procedure was applied for the processing of GRACE and GRACE-FO, as well as for the kinematic orbit solutions of the LEO satellites. The stochastic model was set up independently for each observation type and month in an iterative procedure, as part of a least-squares adjustment of the gravity field, estimated to a maximum degree and order of 96 to reduce computation time. This stochastic information about the observations was later introduced as a priori information in the fully parameterized least-squares adjustment for the GOCO2025s contributions.

For each month, the respective observations were divided into short arcs with a maximum length of 3 h. The noise of the observations was assumed to be wide-sense stationary, and the correlations of the individual short arcs were neglected. Therefore, the covariance function depends only on the lag within one arc and not on the absolute time. Since the stochastic model was estimated in the spectral domain, the covariance function was represented through its Fourier transform, the power spectral density (Khintchine, 1934; Etten, 2006). The cofactor matrix of each short arc m can therefore be represented as the weighted sum over all frequencies ν through

$$\mathbf{Q}_m = \sum_{\nu=0}^{N_m-1} a_\nu^2 \mathbf{F}_{\nu,m}, \tag{1}$$

where a_ν^2 is the variance and $\mathbf{F}_{\nu,m}$ is the respective cofactor component matrix. The entries of $\mathbf{F}_{\nu,m}$ are defined by the type-I discrete cosine transform (DCT, Rao and Yip, 1990) and depend only on the lag k between two epochs i and j

$$(\mathbf{F}_{\nu,m})_{ij} = \frac{2-\delta_{k,0}-\delta_{k,N_m-1}}{\sqrt{2(N_m-1)}} \cos\left(\frac{\pi \nu k}{N_m-1}\right), \qquad k=|i-j|, \qquad i,j \in \{0,\dots,N_m-1\}. \tag{2}$$

$\mathbf{F}_{\nu,m}$ represents the $N_m \times N_m$ matrix of DCT coefficients, with N_m being the number of epochs in the specific arc m. The unknown variance components a_ν^2 are estimated by frequency-wise VCE, as described in Ellmer (2018).

https://doi.org/10.5194/essd-2026-639
Preprint. Discussion started: 29 September 2026

In the first step, an approximate covariance matrix for each arc $\boldsymbol{\Sigma}_m$ is required. If a priori information about the uncertainties of the observations is known, as it is for the POD-derived kinematic orbits in the form of a 3×3 epoch-wise covariance matrix, it can already be introduced here. Otherwise, the covariance matrix is initialized as an identity matrix, corresponding to a white noise covariance function. As the short arcs m are assumed to be uncorrelated, the accumulated normal equation system

$$\mathbf{N} = \sum_{m=1}^{M} \mathbf{A}_m^T \boldsymbol{\Sigma}_m^{-1} \mathbf{A}_m, \qquad \boldsymbol{n} = \sum_{m=1}^{M} \mathbf{A}_m^T \boldsymbol{\Sigma}_m^{-1} \Delta \boldsymbol{l}_m \tag{3}$$

can be set up, where $\mathbf{A}_m$ is the Jacobian of the reduced observations $\Delta \boldsymbol{l}_m$. Subsequently, the solution of the least-squares adjustment

$$\Delta\hat{\mathbf{x}} = \mathbf{N}^{-1}\boldsymbol{n} \tag{4}$$

can be determined. The quadratic sum of the residuals for each frequency e_ν^2 can then be formed using the residuals for each arc $\hat{\mathbf{e}}_m$ and the respective DCT matrix $\mathbf{F}_{\nu,m}$ through

$$e_\nu^2 = \sum_{m=1}^{M} \hat{\mathbf{e}}_m^T \boldsymbol{\Sigma}_m^{-1} \mathbf{F}_{\nu,m} \boldsymbol{\Sigma}_m^{-1} \hat{\mathbf{e}}_m, \qquad \hat{\mathbf{e}}_m = \Delta\mathbf{l}_m - \mathbf{A}_m \Delta\hat{\mathbf{x}}. \tag{5}$$

Using the redundancies of each frequency

$$r_\nu = \sum_{m=1}^{M} \operatorname{trace}\left[\boldsymbol{\Sigma}_m^{-1} \mathbf{F}_{\nu,m} \boldsymbol{\Sigma}_{\mathbf{m}}{}^{-1} (\boldsymbol{\Sigma}_m - \mathbf{A}_m \mathbf{N}^{-1} \mathbf{A}_m^T)\right], \tag{6}$$

the respective variance

$$a_\nu^2 = \frac{e_\nu^2}{r_\nu} \tag{7}$$

can be estimated. The cofactor matrix $\mathbf{Q}_m$ with the dimension of the respective short arc is then formed using Eq. (1), summing over all frequencies using the estimated variance components. The Toeplitz structure of $\mathbf{Q}_m$ is identical within one month for all arcs of the same length. However, an additional variance factor $\hat{\sigma}_m^2$ is estimated for each arc. Consequently, arcs with flawed data are down-weighted in the adjustment process. For the estimation of $\hat{\sigma}_m^2$, the quadratic sum of the residuals for each arc e_m^2 as well as the redundancy r_m are required. These values can be obtained using Eq. (5) and Eq. (6), but adding up all frequency components for each arc $\sum_{\nu=0}^{N_m-1}$ instead of adding up all arcs for each frequency. The arc-wise variance factor

$$\tilde{\sigma}_m^2 = \frac{e_m^2}{r_m} \tag{8}$$

is intended to describe only the relative weighting of the arcs, since the absolute magnitude of the covariance matrix is already adjusted by a_ν^2. Therefore, $\tilde{\sigma}_m^2$ is divided by a robust mean over all arcs to avoid any double consideration of variance components, resulting in a normalized variance factor $\hat{\sigma}_m^2$. Using $\hat{\sigma}_m^2$ and $\mathbf{Q}_m$, the covariance matrix of the reduced observations for each arc

$$\boldsymbol{\Sigma}_m = \hat{\sigma}_m^2 \mathbf{Q}_m \tag{9}$$

can be obtained and inserted in Eq. (3) for the next iteration.

https://doi.org/10.5194/essd-2026-639
Preprint. Discussion started: 29 September 2026

3.3 Stochastic modeling of background model uncertainties for GRACE and GRACE-FO

Errors in background models mainly affect the long- to medium-wavelength part of the gravity field spectrum. Kvas and Mayer-Gürr (2019) showed that incorporating background model uncertainties into the GRACE gravity field recovery process leads to a more realistic stochastic observation model and further improves the quality of the spherical harmonic coefficients. Compared with the other satellite contributions used for GOCO2025s, the spectral range affected by these uncertainties is dominated by GRACE and GRACE-FO observations. Therefore, the introduction of additional information in the form of background model uncertainties and the corresponding stochastic modeling was performed only for GRACE and GRACE-FO.

The uncertainties of the background models are inherent in the reduced observations of the least-squares adjustment. They can be accounted for by either augmenting the covariance matrix of the observations or by estimating additional model correction terms together with a predefined error model (Kvas and Mayer-Gürr, 2019). For GOCO2025s, the second approach was chosen. Error information from AOD1B RL07 and the LISFLOOD model was used to describe the stochastic properties of short-term non-tidal gravity field changes in atmosphere and ocean, and hydrology, respectively. The stochastic model was determined following the approach from Kvas and Mayer-Gürr (2019), using an AR model.

Within the GRACE and GRACE-FO processing, the short-term gravity changes were parameterized as 6-hourly linear splines of potential coefficients up to degree and order 96. To account for the linear dependency between short-term correction terms and long-term gravity field parameters in a combined least-squares adjustment, pseudo-observations were introduced. These pseudo-observations constrain the correction terms towards zero.

The predefined error model was estimated using the AOe07 error time series and the LISFLOOD model output. First, 6-hourly linear splines of spherical harmonics up to degree and order 96 were generated to align the input data with the parametrization of the model corrections. Subsequently, the static, trend, annual, and semi-annual parts of the signal were reduced. The actual realization of the error process was then defined as the weighted sum of the AOe07 and the LISFLOOD time series

$$\boldsymbol{y}_e = \boldsymbol{y}_{\mathrm{AOe07}} + 0.5\boldsymbol{y}_{\mathrm{LF}}. \tag{10}$$

Since at the time of processing there was no error information about the LISFLOOD model available, the rudimentary assumption of 50 % of the signal being noise was made. Also, $\boldsymbol{y}_e$ was assumed to represent a stationary random error process, and therefore its covariance function only depends on the lag k. Consequently, the covariance matrix of the background model uncertainties $\boldsymbol{\Sigma}_{\boldsymbol{y}_m}$ has a block-Toeplitz structure, where each block corresponds to the covariance matrix at a specific lag. Due to numerical instabilities at higher lags when directly determining $\boldsymbol{\Sigma}_{\boldsymbol{y}_m}$, the stochastic process is approximated by a vector AR model of order $p = 3$. Such a process is completely defined by its coefficient matrices $\boldsymbol{\Phi}^{(p)}$ and its white noise covariance matrix $\boldsymbol{\Sigma}_w^{(p)}$ (Lütkepohl, 2013). These matrices can be obtained by solving the Yule–Walker equation for multivariate AR processes using empirical covariance matrices derived from the unbiased estimator

$$\boldsymbol{\Sigma}_k = \frac{1}{N-k}\sum_{i=1}^{N-k} \boldsymbol{y}_{e_{i+k}} \boldsymbol{y}_{e_i}^T \tag{11}$$

https://doi.org/10.5194/essd-2026-639
Preprint. Discussion started: 29 September 2026

Open Access Earth System Science Data Discussions

for the lags $k = 0, \ldots, p_{max}$, where N denotes the total number of the error samples. Since the parameter dimension is too large for a stable estimation of $\mathbf{\Sigma}_k$ at a spatial resolution up to degree and order 96 and a temporal resolution of 6-hourly time splines, the covariance matrices were projected onto a reduced basis obtained from an eigenvalue decomposition. Only the eigenvectors corresponding to the 500 largest eigenvalues, evaluated in terms of gravity disturbances at 500 km satellite altitude, were retained. The empirical covariance matrices for all lags were then used to estimate the AR model coefficients according to

$$\mathbf{\Sigma}_k = \sum_{j=1}^{p} \mathbf{\Phi}_j^{(p)} \mathbf{\Sigma}_{k-j}. \tag{12}$$

The corresponding white noise covariance matrix is given by

$$\mathbf{\Sigma}_w^{(p)} = \mathbf{\Sigma}_0 - \sum_{j=1}^{p} \mathbf{\Phi}_j^{(p)} \mathbf{\Sigma}_j^T. \tag{13}$$

To mitigate warm-up effects, which are introduced for epochs smaller than $p = 3$, AR models of order $p = 0, 1, 2$ were additionally derived. The lower-order AR coefficients were then inserted at the corresponding positions, resulting in the block matrix

$$\mathbf{\Phi} = \begin{bmatrix} \mathbf{I} & & & & & \\ -\mathbf{\Phi}_1^{(1)} & \mathbf{I} & & & & \\ -\mathbf{\Phi}_2^{(2)} & -\mathbf{\Phi}_1^{(2)} & \mathbf{I} & & & \\ -\mathbf{\Phi}_3^{(3)} & -\mathbf{\Phi}_2^{(3)} & -\mathbf{\Phi}_1^{(3)} & \mathbf{I} & & \\ & -\mathbf{\Phi}_3^{(3)} & -\mathbf{\Phi}_2^{(3)} & -\mathbf{\Phi}_1^{(3)} & \mathbf{I} & \\ & & \ddots & \ddots & \ddots & \ddots \end{bmatrix}. \tag{14}$$

Together with the block-diagonal covariance matrix of the resulting white noise sequence Σ_w, the inverse covariance matrix of the background model uncertainties is given by

$$\mathbf{\Sigma}_{\boldsymbol{y}_m}^{-1} = \mathbf{\Phi}^T \mathbf{\Sigma}_w^{-1} \mathbf{\Phi}. \tag{15}$$

This prior information was then included in the normal equations of the monthly GRACE and GRACE-FO solutions.

3.4 SLR normal points

The least-squares adjustment for SLR is based on a modified Huber estimator, which iteratively down-weights observations with large outliers using VCE (Süsser-Rechberger et al., 2026). Since SLR stations operate with different levels of accuracy, a station-specific adjustment factor was determined as well. The ultimate weight of a single normal point observation i was then derived by the inverse of the squared standard deviation

$$\hat{\sigma}_i = \hat{\sigma}_i^{\text{Huber}} \hat{\sigma}^{\text{stat}} \hat{\sigma}_{\text{apriori}}^{\text{stat}}. \tag{16}$$

https://doi.org/10.5194/essd-2026-639
Preprint. Discussion started: 29 September 2026

Here, $\hat{\sigma}^{\text{stat}}_{\text{apriori}}$ is an a priori factor for the station accuracy, as it is provided in the normal point data files. $\hat{\sigma}_i^{\text{Huber}}$ and $\hat{\sigma}^{stat}$ were determined iteratively from the residuals, down-weighting each observation and adjusting the station-specific scale factor, respectively.

4 Combination process of GOCO2025s

The combined normal equation system of GOCO2025s was obtained by accumulating the normal equations of the individual satellite contributions $s \in$ {GOCE, GRACE, GRACE-FO, kinematic orbits, SLR}, together with the regularization applied to the static part, the trend, the annual, and the semi-annual variations of the gravity field:

$$\mathbf{N} = \sum_s \frac{1}{\sigma_s^2}\mathbf{N}_s + \frac{1}{\sigma^2_{\text{static}}}\mathbf{N}_{\text{Kaula}} + \boldsymbol{\Sigma}^{-1}_{\Omega_{\text{trend}}} + \boldsymbol{\Sigma}^{-1}_{\Omega_{1\text{yr}}} + \boldsymbol{\Sigma}^{-1}_{\Omega_{0.5\text{yr}}}, \quad \boldsymbol{n} = \sum_s \frac{1}{\sigma_s^2}\boldsymbol{n}_s. \tag{17}$$

The normal equations of the satellite contributions and the regularization of the static part were weighted using the inverse of the respective variance factors, which were estimated in an iterative procedure using VCE. The individual normal equation matrices $\mathbf{N}_*$ were zero-padded to account for the different parametrization of each contribution and to match the dimension of the combined normal equation matrix $\mathbf{N}$. Since the stochastic modeling of the individual satellite contribution was already inherent in the respective normal equation, the value of each variance factor σ_*^2 was very close to 1. The employed regularization stabilizes the solution by suppressing the noise of higher-degree spherical harmonics. For this purpose, a Kaula-type signal covariance model in the form of $\mathbf{K} = \text{diag}(10^{-10} n^{-2\alpha})$ was used for the regularization of the static part of the gravity field. This regularization was applied for degrees $n = 150, \cdots, 300$, with $\alpha = 2$. The corresponding normal equation is then given by

$$\mathbf{N}_{\text{Kaula}} = \mathbf{K}^{-1}. \tag{18}$$

For the temporal variations, an adapted Kaula-type regularization $\boldsymbol{\Sigma}_\Omega$ was implemented following the approach from Kvas et al. (2021), accounting for regionally varying signal levels. The signal covariance model for the trend was determined separately for the regions $r \in$ {Antarctica, Greenland, Iceland, rest of the continents, Caspian Sea, ocean}, while the signal covariance model for the annual and semi-annual variations was separated into $r \in$ {land, ocean}. The regularization of the temporal variations was applied from degree 2 to 200, with $\alpha = 2.1$ for land areas, including the Caspian Sea, and $\alpha = 2.25$ for the ocean. To determine the regularization matrix $\boldsymbol{\Sigma}_\Omega$, a window matrix for each region

$$\mathbf{W}_{\Omega_r} = (\mathbf{S}^T\mathbf{S})^{-1}\mathbf{S}^T\mathbf{D}_{\Omega_r}\mathbf{S} \tag{19}$$

was first set up in the spherical harmonics domain. This was done using the spherical harmonic synthesis matrix $\mathbf{S}$, which maps the potential coefficients from degree 2 to 200 to values on a grid using a water height kernel. $\mathbf{D}_{\Omega_r}$ is a window matrix in the spatial domain containing smoothed grid values between 0 and 1, obtained using a Gaussian filter with a smoothing radius of 120 km. The term $(\mathbf{S}^T\mathbf{S})^{-1}\mathbf{S}^T$ represents the least-squares spherical harmonic analysis, which transforms the grid values back

https://doi.org/10.5194/essd-2026-639
Preprint. Discussion started: 29 September 2026

to spherical harmonic coefficients. The regularization matrix for the temporal variations is then defined as the sum over the respective regions:

$$\boldsymbol{\Sigma}_\Omega = \sum_r \sigma^2_{\Omega_r} \mathbf{W}_{\Omega_r} \mathbf{K} \mathbf{W}^T_{\Omega_r} = \sum_r \sigma^2_{\Omega_r} \mathbf{V}_{\Omega_r}. \tag{20}$$

Here, the Kaula-type signal covariance model $\mathbf{K}$, using the respective land or ocean value of α, is localized by the regional window matrix $\mathbf{W}_{\Omega_r}$. The signal level of the respective region $\sigma^2_{\Omega_r}$ was estimated using VCE in the least-squares adjustment according to

$$\sigma^2_{\Omega_r} = \frac{\hat{\boldsymbol{x}}^T \boldsymbol{\Sigma}_\Omega^{-1} \mathbf{V}_{\Omega_r} \boldsymbol{\Sigma}_\Omega^{-1} \hat{\boldsymbol{x}}}{\operatorname{trace}\left[(\boldsymbol{\Sigma}_\Omega^{-1} - \boldsymbol{\Sigma}_\Omega^{-1} \mathbf{N}^{-1} \boldsymbol{\Sigma}_\Omega^{-1}) \mathbf{V}_{\Omega_r}\right]}. \tag{21}$$

In this equation, $\boldsymbol{\Sigma}_\Omega$ and $\mathbf{V}_{\Omega_r}$ were zero-padded to match the dimension of the estimated solution vector $\hat{\boldsymbol{x}}$ and the combined normal equation matrix $\mathbf{N}$. To preserve the phase of the periodic signal, a common signal level factor was estimated for the sine and cosine coefficients of the annual and semi-annual variations, respectively. The structure of the combined normal equation matrix $\mathbf{N}$ is illustrated in Fig. 1.

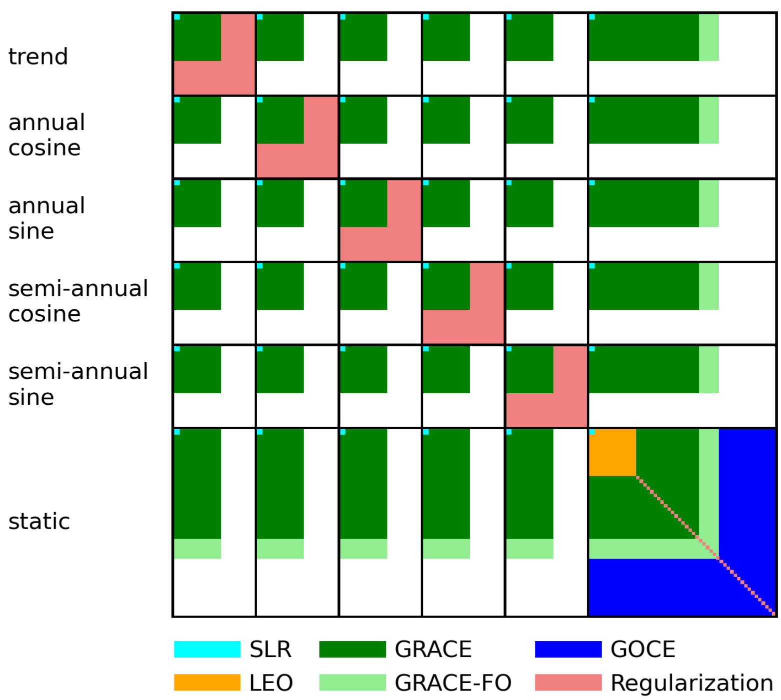

Figure 1. Schematic structure of the combined GOCO2025s normal equation matrix N, showing the overlaid contributions of the individual observation techniques and the applied regularization. The matrix is ordered degree-wise according to the estimated temporal and static gravity field parameters. All contributions are shown up to scale, except for the regularization of the static gravity field.

https://doi.org/10.5194/essd-2026-639
Preprint. Discussion started: 29 September 2026

Open Access Earth System Science Data Discussions

4.1 Contribution of individual components

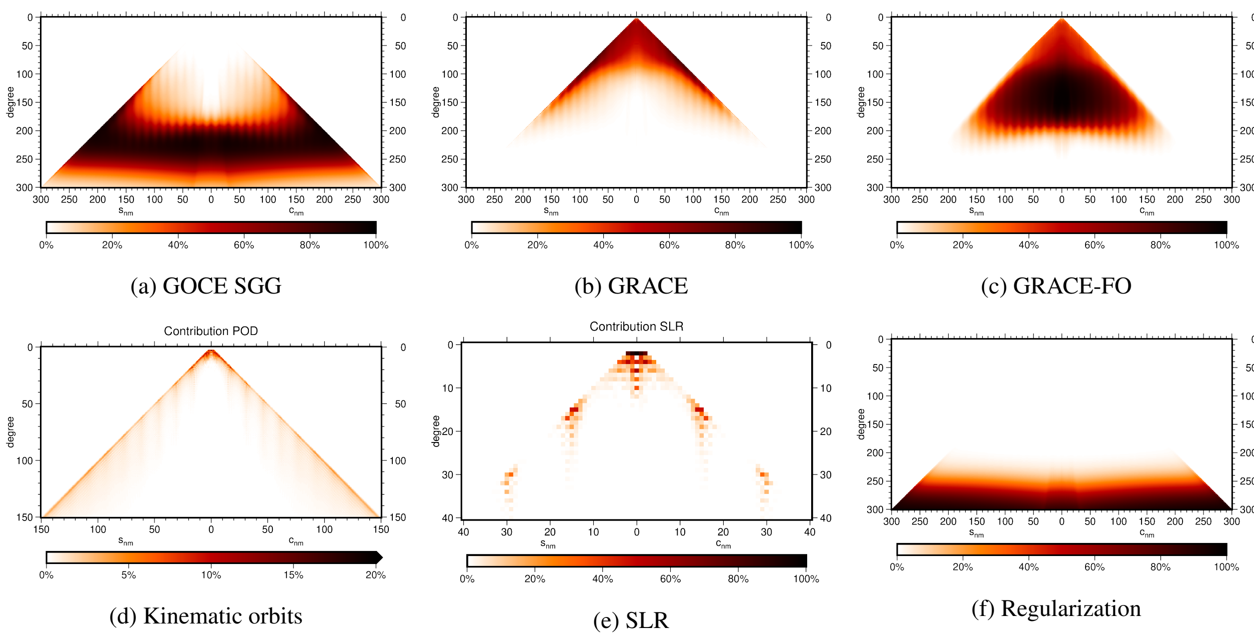

(a) GOCE SGG (b) GRACE (c) GRACE-FO (d) Kinematic orbits (e) SLR (f) Regularization

Figure 2. Contribution of GOCE, GRACE, GRACE-FO, kinematic orbits, SLR, and the Kaula regularization to the GOCO2025s potential coefficients of the static field. Note the different axis limits in panels (d) and (e), as well as the different color scale used in panel (d).

When solving the combined normal equation system, the contribution of each normal equation component can be assessed by forming the redundancy matrix

$$\mathbf{R}_* = \frac{1}{\sigma_*^2}\mathbf{N}_*\mathbf{N}^{-1} \tag{22}$$

using the combined normal equation matrix $\mathbf{N}$ and the individual normal equation matrix $\mathbf{N}_*$ for GOCE, GRACE, GRACE-FO, the kinematic orbits, SLR, or the regularization. The information on how much each component contributes relatively to the combined solution is inherent in the diagonal elements of $\mathbf{R}_*$. The coefficient triangles in Fig. 2 show the individual contributions of the different techniques to the specific parts of the spherical harmonic spectrum of the static gravity field.

As expected, GOCE contributes most to the high-degree spherical harmonics, particularly from degree 180 to 270, due to its low orbital altitude and the sensitivity of satellite gravitational gradiometry (Brockmann et al., 2021). The polar gap of GOCE is largely compensated for by GRACE-FO, as indicated by the contribution to the near-zonal spherical harmonics. Conversely, the resonance orders of GRACE and GRACE-FO (Cheng and Ries, 2017), which appear as multiples of 15 with reduced impact on the solution, are compensated for by GOCE. The GRACE and GRACE-FO normal equations provide the largest contribution to the spherical harmonics up to degree 200. Interestingly, the impact of GRACE-FO is considerably larger than that of GRACE, despite the fact that only about 6 years of GRACE-FO data were used compared to approximately 14 years of GRACE data. This can be attributed to the significantly higher measurement precision of the LRI compared to the KBR instrument. The enhanced processing strategy of using both ranging systems for GRACE-FO and the underlying stochastic modeling is particularly beneficial for the determination of the near-zonal and tesseral spherical harmonics of degree 70 to 200. SLR is suitable only for the determination of the very-low-degree coefficients due to the sparse distribution of SLR stations and the small number of observations. This can also be seen in the coefficient triangles, as SLR contributes primarily to the degree 2 coefficients, to even zonal coefficients up to degree 10, and partly to some near-sectorial coefficients around degrees 15 and 30. The kinematic orbits of the LEO satellites play a minor role in the GOCO2025s combination. Their contribution is mainly limited to coefficients up to degree 10 and, to some extent, to the near-sectoral coefficients up to degree 150. The regularization of the static part of the gravity field contributes primarily to the coefficients from degree 250 to 300, where the noise level becomes increasingly dominant.

5 Results

In this section, the GOCO2025s model is evaluated using independent data sets, including GNSS, leveling, and altimetry. The performance of GOCO2025s is assessed relative to the previous models of the GOCO series (see Fig. 3) and other state-of-the-art global gravity field models. The validation for the long-wavelength part of GOCO2025s is performed by analyzing orbit residuals between numerically integrated orbits and kinematic orbits derived from GPS observations. Over land, the short-wavelength performance is assessed by comparing model-derived geoid heights against geoid height derived from GNSS and leveling at GNSS stations distributed over several regions worldwide. Over the oceans, the short-wavelength part of the model is validated against altimetry-derived gravity anomalies.

5.1 Orbit residuals

The low-degree spherical harmonic coefficients of the GOCO2025s model were evaluated by comparing the reduced dynamic orbits from GRACE-FO, Sentinel 1A/1C/2A/2B/3A/3B/6A and Swarm A/B/C against the corresponding GPS-derived kinematic orbit positions for January 2025. Since kinematic orbits from 2025 were not considered in the determination of GOCO2025s, this provides an independent validation of the model.

Dynamic orbits were integrated following the strategy outlined in Ellmer and Mayer-Gürr (2017), using the background models from Table 2. Subsequently, these orbits were fitted to the kinematic orbit observations described in Sect. 2.4. In this least-squares adjustment, empirical satellite-specific acceleration parameters were estimated together with the initial states of the integrated orbits. For GRACE-FO, an accelerometer bias in terms of cubic splines with a sampling of 6 h and a fully-populated constant daily scale matrix were parameterized. For the Sentinel satellites, the bias was represented by cubic splines with a sampling of 1.5 h, and once-per-revolution empirical accelerations were estimated in along-track, cross-track, and radial directions The empirical acceleration parameterization used for Swarm was identical to the one applied for the Sentinel satellites.

The orbit residuals were determined in the same way for all gravity field models. For each comparison, only the spherical harmonic coefficients were replaced, while the remaining processing strategy was kept unchanged. GOCO2025s, including

https://doi.org/10.5194/essd-2026-639
Preprint. Discussion started: 29 September 2026

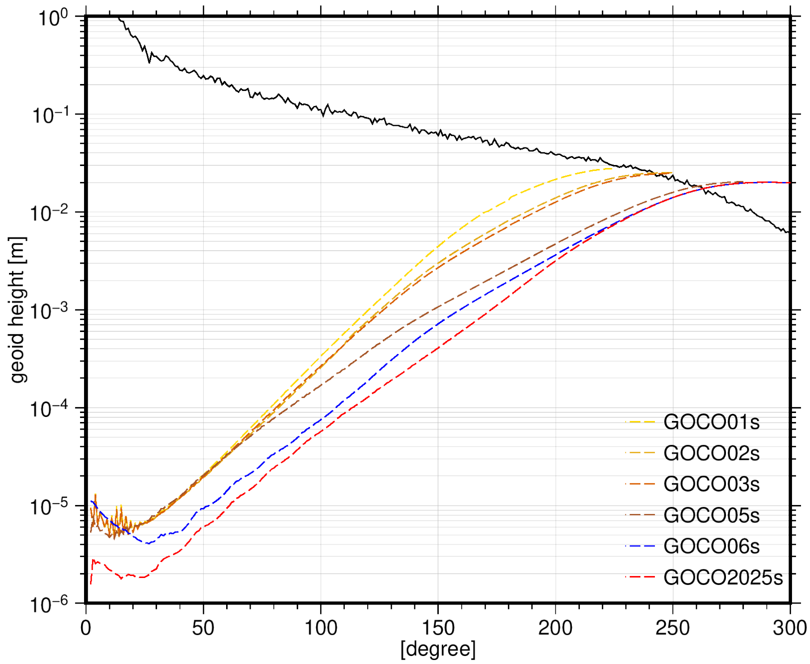

Figure 3. Formal errors of all GOCO releases in the form of geoid heights up to their respective maximum spherical harmonic degree.

trend, annual- and semi-annual variations, was evaluated against GOCO06s, including trend and annual variations, and against the monthly ITSG operational gravity field solution. ITSG operational denotes the up-to-date monthly gravity field solutions provided by the Institute of Geodesy at TUG. Since both GOCO06s and ITSG operational are consistent with AOD1B RL06, modified versions of these models were used to ensure consistency with the AOD1B RL07 model applied in this validation. The assessment of the orbit accuracy was carried out for January 2025, using these three gravity field models.

As shown in Table 3, GOCO2025s consistently outperforms its predecessor GOCO06s in terms of monthly root mean square (RMS) orbit residuals. As expected, ITSG operational yields the lowest RMS values. This can be attributed to the fact that ITSG operational contains actual GRACE-FO observations for January 2025, whereas the GOCO models were extrapolated to this month using their estimated temporal parametrization. Nevertheless, the orbit accuracy improves substantially when GOCO2025s is used instead of GOCO06s, indicating an enhanced long-wavelength part of the new GOCO release.

5.2 Comparison with GNSS/leveling

Global gravity field models can be validated over land by comparing model-derived geoid heights or height anomalies against independent height information obtained from GNSS observations and leveling. For this type of validation, the satellite-based and ground-based quantities must be consistent in terms of signal content and height system definition in order to avoid systematic errors. Ground-based geoid heights or height anomalies are derived by subtracting orthometric or normal heights determined by leveling from geometric heights above the reference ellipsoid as obtained by GNSS. Since these quantities are

https://doi.org/10.5194/essd-2026-639
Preprint. Discussion started: 29 September 2026

Table 3. 3D RMS differences between reduced-dynamic orbits integrated using the respective gravity field models and the kinematic orbits for January 2025.

	GOCO06s	GOCO2025s	ITSG op.
GRACE-FO 1	1.80	1.09	0.83
GRACE-FO 2	1.78	1.10	0.85
Sentinel 1a	2.45	2.12	2.08
Sentinel 1c	1.75	1.41	1.36
Sentinel 2a	4.45	4.22	4.20
Sentinel 2b	4.27	4.03	3.96
Sentinel 2c	2.91	2.63	2.47
Sentinel 3a	3.71	3.48	3.41
Sentinel 3b	3.65	3.43	3.36
Sentinel 6a	1.06	0.93	0.91
Swarm A	25.45	25.18	25.02
Swarm B	15.72	15.57	15.63
Swarm C	34.43	34.30	34.14

observed at the Earth's surface, they contain gravity field signal beyond the spectral resolution of truncated global models. When geoid heights or height anomalies are computed from global gravity field models, the signal content is limited by the maximum spherical harmonic degree of the respective model. The missing high-frequency signal is referred to as omission error. This omitted signal has to be accounted for when comparing model-derived quantities with GNSS/leveling-derived height information. Usually, independent high-resolution gravity field models are used to estimate the omission error, which is then removed from the GNSS/leveling-derived quantities. A detailed description of geoid comparisons using gravity field models and ground-based observations is given in Gruber et al. (2011).

The validation of GOCO2025s was performed using height data sets derived from GNSS/leveling for several regions and comparing the results with other global gravity field models. Geoid height or height anomaly differences were determined for GNSS stations in Australia, Austria, Brazil, Germany, the USA, and Switzerland (see Table 4). For each region, a planar correction surface was computed and removed from the differences to account for inconsistencies in the height system definitions.

Besides the predecessors of GOCO2025s (GOCO01s, GOCO02s, GOCO03s, GOCO05s and GOCO06s), the satellite-only models Tongji-GMMG2021S (Chen et al., 2018, 2022; Tongji, 2021) and WHU-SWPU-GOGR2022S (Zhao et al., 2023) were included in the assessment. In addition, the combined models XGM2019 (Zingerle et al., 2019, 2020) and SGG-UGM-2 (Liang et al., 2020), which incorporate terrestrial gravity data, were used for comparison. All satellite-only models are based on GRACE and GOCE observations, while the GOCO series additionally includes a varying number of kinematic orbits and

https://doi.org/10.5194/essd-2026-639
Preprint. Discussion started: 29 September 2026

Table 4. Overview of the utilized GNSS/leveling data sets.

Country	Number of points	Reference
Australia	7627	Featherstone et al. (2018)
Austria	54	Bundesamt für Eich- und Vermessungswesen (2016)
Brazil	1180	Brazilian Institute of Geography and Statistics (2019)
Germany	470	GeoBasis-DE/Geobasis NRW (2018)
USA	222	National Geodetic Survey; van Westrum et al. (2021)
Switzerland	206	swisstopo (2016)

SLR observations to different satellites, and GOCO2025s further uses GRACE-FO data. XGM2019 and SGG-UGM-2 combine satellite gravimetry and altimetry data with terrestrial gravity observations.

For the comparison, each model was truncated in 10 degree steps from spherical harmonic degree and order 10 up to 300. Above the respective truncation degree, the omission error was computed up to degree and order 2190 using the high-resolution gravity field models EGM2008 (Pavlis et al., 2012) and ERTM2160 (Hirt et al., 2014). Figure 4 shows the RMS of the geoid height or height anomaly differences for all truncation degrees of the selected global gravity field models and the individual GNSS/leveling data sets for each specific region. The gravity field models, XGM2019 and SGG-UGM-2, provide a useful reference level for the performance that can be achieved when satellite data are supplemented by terrestrial and altimetry-derived gravity observations. GOCO2025s is therefore primarily assessed relative to the other satellite-only models.

The general shape of the RMS curves shown in Figure 4 is similar for all investigated regions, with the exception of Brazil. For Brazil, the RMS values decrease markedly around degree 100. This is an indication of low quality of the terrestrial data used in EGM2008 over this region. This interpretation is supported by the fact that models including GOCE data show improved performance at higher truncation degrees, resulting in lower RMS values than those obtained when using EGM2008 for the omission error. The RMS curves of the satellite-only models deviate from the error level of the combined models at different spatial scales. This is an indication of the maximum spherical harmonic degree up to which reliable signal content is present in the respective model. The observed behaviour is in accordance with the part of the spherical harmonic spectrum where the regularization contributes most to the determination of the coefficients (compare Figure 2f for GOCO2025s).

With regard to the previous GOCO models, a higher version number indicates an increase in satellite data. GOCO01s, GOCO02s and GOCO03s are based on 7.5 years of GRACE observations, while the impact of the increasing amount of GOCE data is clearly visible. These models include two, eight, and 18 months of GOCE gradiometry data, respectively. From GOCO05s onwards, the complete GOCE time series was used, together with 10.5 years of GRACE data for GOCO05s and an almost complete GRACE time series for GOCO06s and GOCO2025s (see the GOCO website[2] for more information). WHU-SWPU-GOGR2022s and Tongji-GMMG2021s also use nearly the complete GRACE and GOCE observation periods.

All analyzed satellite-only models start to diverge from the combined models by degree 200 at the latest. GOCO06s and GOCO2025s show very similar behaviour at high degrees, which is expected because the same GOCE SGG normal equations

[2]https://www.asg.ed.tum.de/iapg/forschung/schwerefeld/goco/

https://doi.org/10.5194/essd-2026-639
Preprint. Discussion started: 29 September 2026

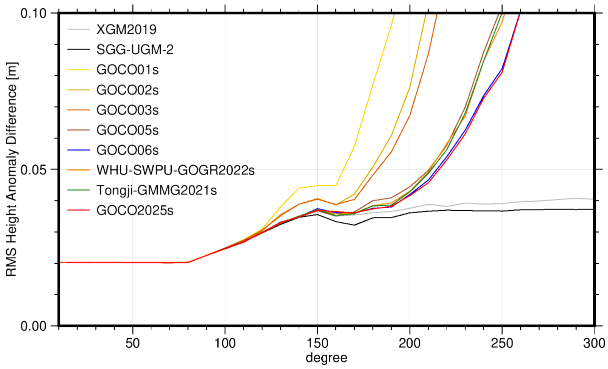

(a) Australia (7627 points)

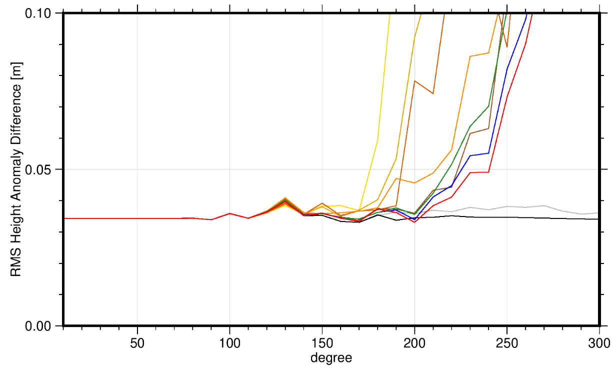

(b) Austria (54 points)

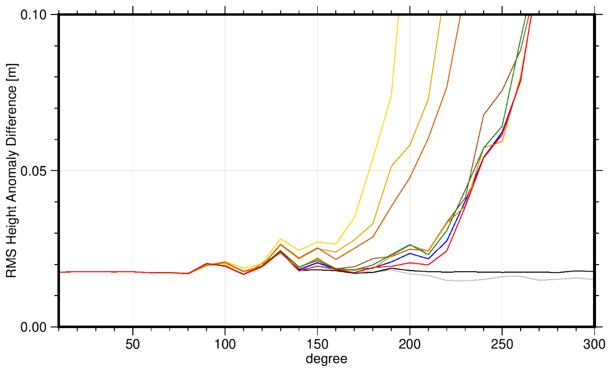

(c) Germany (470 points)

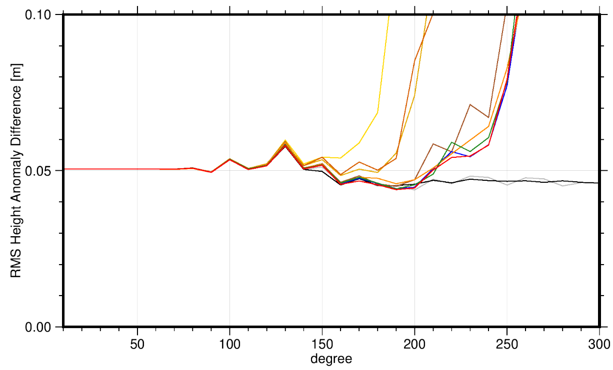

(d) Switzerland (206 points)

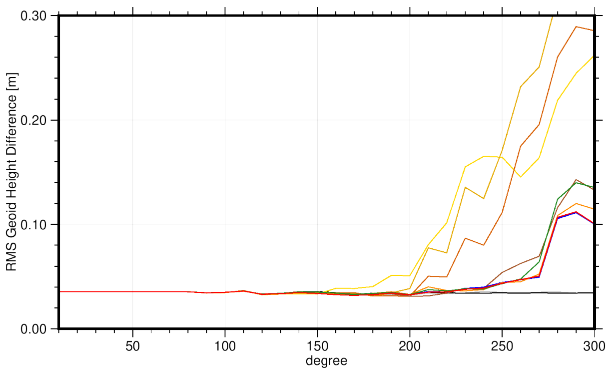

(e) USA (222 points)

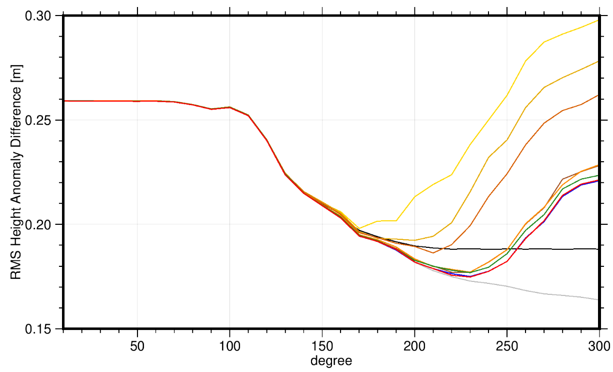

(f) Brazil (1180 points)

Figure 4. RMS of the difference between model-derived and GNSS/leveling-derived geoid heights or height anomalies in meters for each truncation degree. Note the different scale for USA and Brazil.

https://doi.org/10.5194/essd-2026-639
Preprint. Discussion started: 29 September 2026

were used in both models. In the medium degree range, GOCO2025s shows improved performance, which is particularly evident for the German and Austrian data sets. This improvement can be attributed to the inclusion of GRACE-FO data and the high measurement precision of the LRI instrument. Overall, GOCO2025s performs best among the analyzed satellite-only models, yielding the lowest RMS values with respect to the GNSS/leveling data.

5.3 Comparison with altimetry data

To evaluate the short-wavelength part of GOCO2025s over ocean areas, gravity anomalies derived from the model were compared with version 33.1 of the global $1' \times 1'$ gravity anomaly grid developed by the Scripps Institution of Oceanography (Sandwell et al., 2014). This data set, hereafter referred to as SIO33.1, is based on multi-mission satellite altimetry, including observations from Altika, Cryosat, Envisat, Jason-1/2 and Sentinel-3A/B, and is available via the Scripps Institution of Oceanography data portal[3].

For validation, GOCO2025s was extended from degree and order 300 to 2190 using EGM2008. The normal gravity field based on GRS80 (Moritz, 1980) was reduced up to degree 10 before gravity anomalies were computed on the $1' \times 1'$ grid. The differences between the two gravity anomaly data sets were subsequently averaged to a $30' \times 30'$ grid to approximately match the spatial resolution corresponding to degree and order 300 of the original GOCO2025s model. Land areas were excluded, and the global RMS of the residual gravity anomalies was used as the validation metric. As shown in Figure 5, the two gravity anomaly data sets agree quite well over most ocean areas. The largest residuals occur mainly in regions characterized by strong short-wavelength gravity signals and in dynamically active ocean regions. For comparison, the same procedure was applied to GOCO06s. The global RMS values with respect to SIO33.1 are 5.97 mGal for GOCO2025s and 5.98 mGal for GOCO06s. This difference is not significant, indicating that the same signal content is present in both models. Nevertheless, GOCO2025s yields a slightly lower RMS value when compared to the independent altimetry-derived gravity anomalies than GOCO06s.

6 Data availability

The global satellite-only gravity field model GOCO2025s is available at the TUG Repository as well as on the International Centre for Global Earth Models (ICGEM, Ince et al., 2019) website and is identified with the following DOI: 10.3217/f48p8-8h651 (Öhlinger et al., 2025). The individual files of GOCO2025s on the TUG Repository contain the static gravity field coefficients up to degree and order 300, the constrained secular, annual, and semi-annual variations up to degree and order 200 and their respective uncertainty information in "GOCO2025s.gfc"; All parts of the normal equation system of the static gravity field, including the original normal equation, the vector of the right hand side, apriori values of the unknown parameters, the normal equation of the applied constraints and the resulting solution vector in "GOCO2025s_normalEquation.snx"; and the gravitational potential of non-tidal atmospheric and ocean masses already included in GOCO2025s for the AOD1B releases RL06 and RL07 in "AOD1B_RL0X_included_in_GOCO22025s.gfc". An algorithm on how to compute a gravity field

[3]https://topex.ucsd.edu/pub/global_grav_1min/

https://doi.org/10.5194/essd-2026-639
Preprint. Discussion started: 29 September 2026

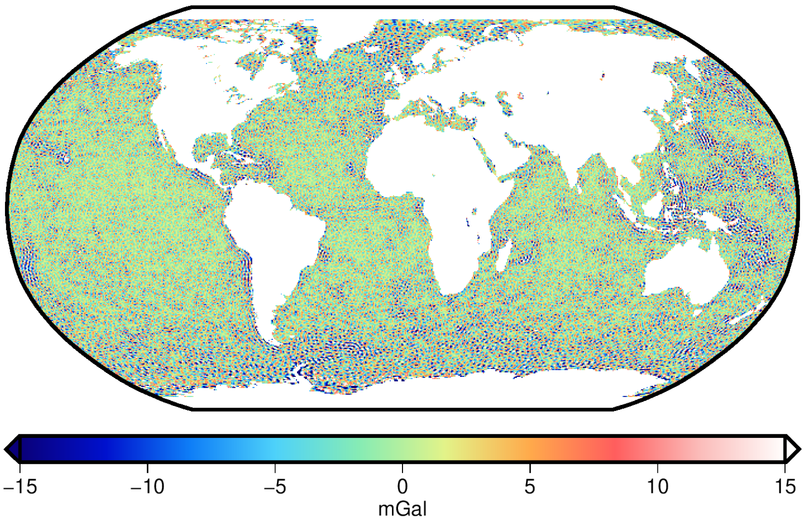

Figure 5. Difference between GOCO2025s-dervied gravity anomalies and SIO33.1 on a $30' \times 30'$ grid in mGal. Land areas are excluded.

functional at a specific time, as well as the procedure on how to use GOCO2025s together with the AOD1B data, is provided in the header of the respective files. On ICGEM, only the primary model data "GOCO2025s.gfc" is published.

7 Conclusions

The GOCO2025s global gravity field model combines GOCE, GRACE, GRACE-FO, kinematic orbit, and SLR data, together with a refined Kaula-type regularization at the normal equation level. The relative weighting was determined using VCE and supported by dedicated stochastic models for each satellite contribution. The analyses have shown that the inclusion of LRI data from GRACE-FO has a particularly strong impact on the quality of the spherical harmonic coefficients between degrees 70 and 200, which can be attributed to the high measurement accuracy of the instrument. The overall quality of GOCO2025s benefits from the complementary sensitivity of the incorporated satellite observation techniques over different parts of the spherical harmonic spectrum. Their combination therefore results in a highly accurate and spectrally balanced representation of the Earth's gravity field. Validation against independent data sets comprising GNSS, leveling, and altimetry in terms of orbit residuals, geoid heights, and gravity anomalies demonstrates that GOCO2025s was further improved compared to the previous models of the GOCO series. In the performed validation tests, GOCO2025s generally outperformed its predecessors and other selected state-of-the-art gravity field models. GOCO2025s provides realistic uncertainty information in the form of standard deviations of the spherical harmonic coefficients, as well as the complete system of unconstrained normal equations. The model is made available to the user community via the TUG repository and the ICGEM website and is intended to support scientific studies and further combinations with gravity field data.

https://doi.org/10.5194/essd-2026-639
Preprint. Discussion started: 29 September 2026

Author contributions. FÖ processed the GRACE and GRACE-FO normal equations, performed the orbit validation and the comparison with altimetry data over ocean areas, and wrote the manuscript. TMG processed the normal equations of the kinematic LEO orbits, SLR, the regularization, and performed the combination of all contributions. BSR implemented the SLR functionality in GROOPS. JMB computed the GOCE normal equations. JN performed the comparison with GNSS leveling. SK and AS refined the non-gravitational force modeling in GROOPS. PD contributed with his expertise in GNSS processing and AR process modeling. TMG and SK acted as scientific advisors.

Competing interests. The authors declare that they have no conflict of interest.

Acknowledgements. The authors gratefully acknowledge all the institutions for providing high-quality input data, particularly ESA for providing GOCE, SWARM, and Sentinel data; the GFZ Information System and Data Center for publishing GRACE, GRACE-FO, CHAMP, TerraSAR-X, and Tandem-X data; AEI for providing LRI L1B data for GRACE-FO; and ILRS for providing SLR measurements. The collaboration between TUG, TUM, and GFZ was greatly appreciated for establishing the MIXED2025 ocean tide model and for providing the AOD1B and LISFLOOD data sets. AI-based language tools were used solely to assist with grammar, spelling, and sentence-structure revisions. The scientific content, interpretation, and conclusion remain the responsibility of the authors. Finally, the authors would like to thank everyone who has contributed to GROOPS' functionality.

References

Altamimi, Z., Rebischung, P., Collilieux, X., Métivier, L., and Chanard, K.: ITRF2020: an augmented reference frame refining the modeling of nonlinear station motions, Journal of Geodesy, 97, https://doi.org/10.1007/s00190-023-01738-w, 2023.

Barthelmes, F.: Definition of Functionals of the Geopotential and Their Calculation from Spherical Harmonic Models, Tech. rep., Deutsches GeoForschungszentrum (GFZ), https://doi.org/10.2312/GFZ.b103-0902-26, 2013.

Behzadpour, S.: Contributions to GRACE/GRACE-FO Time-variable Gravity Field Recovery: Detection and Mitigation of Systematic Errors and Improved Single Accelerometer Approach, Ph.D. thesis, Graz University of Technology, https://doi.org/10.3217/20k8w-91d53, 2022.

Behzadpour, S., Mayer-Gürr, T., and Krauss, S.: GRACE Follow-On Accelerometer Data Recovery, Journal of Geophysical Research: Solid Earth, 126, https://doi.org/10.1029/2020JB021297, 2021.

Brockmann, J. M.: On High Performance Computing in Geodesy - Applications in Global Gravity Field Determination, Ph.D. thesis, University of Bonn, https://nbn-resolving.org/urn:nbn:de:hbz:5n-38608, 2014.

Brockmann, J. M., Schubert, T., Mayer-Gürr, T., and Schuh, W.-D.: The Earth's gravity field as seen by the GOCE satellite - an improved sixth release derived with the time-wise approach (GO_CONS_GCF_2_TIM_R6), GFZ Data Services [data set], https://doi.org/https://doi.org/10.5880/ICGEM.2019.003, 2019.

Brockmann, J. M., Schubert, T., and Schuh, W. D.: An Improved Model of the Earth's Static Gravity Field Solely Derived from Reprocessed GOCE Data, Surveys in Geophysics, 42, 277–316, https://doi.org/10.1007/s10712-020-09626-0, 2021.

Bruinsma, S. and Boniface, C.: The operational and research DTM-2020 thermosphere models, Journal of Space Weather and Space Climate, 11, https://doi.org/10.1051/swsc/2021032, 2021.

Carrere, L., Lyard, F., Cancet, M., Allain, D., Dabat, M.-L., Fouchet, E., Sahuc, E., Faugere, Y., Dibarboure, G., and Picot, N.: A new barotropic tide model for global ocean: FES2022, AVISO [data set], https://doi.org/10.24400/527896/a01-2024.004, presented at the 2022 Ocean Surface Topography Science Team Meeting: https://doi.org/10.24400/527896/a03-2022.3287, 2022.

Chen, J., Zhang, X., Chen, Q., Shen, Y., and Nie, Y.: Static Gravity Field Recovery and Accuracy Analysis Based on Reprocessed GOCE Level 1b Gravity Gradient Observations, https://doi.org/10.5194/egusphere-egu22-6771, 2022.

Chen, Q., Shen, Y., Francis, O., Chen, W., Zhang, X., and Hsu, H.: Tongji-Grace02s and Tongji-Grace02k: High-Precision Static GRACE-Only Global Earth's Gravity Field Models Derived by Refined Data Processing Strategies, Journal of Geophysical Research: Solid Earth, 123, 6111–6137, https://doi.org/10.1029/2018JB015641, 2018.

Cheng, M. and Ries, J.: The unexpected signal in GRACE estimates of C20, Journal of Geodesy, 91, 897–914, https://doi.org/10.1007/s00190-016-0995-5, 2017.

Daras, I., March, G., Pail, R., Hughes, C. W., Braitenberg, C., Güntner, A., Eicker, A., Wouters, B., Heller-Kaikov, B., Pivetta, T., and Pastorutti, A.: Mass-change And Geosciences International Constellation (MAGIC) expected impact on science and applications, Geophysical Journal International, 236, 1288–1308, https://doi.org/10.1093/gji/ggad472, 2024.

De Roo, A. P. J., Wesseling, C. G., and Van Deursen, W. P. A.: Physically based river basin modelling within a GIS: the LISFLOOD model, Hydrological Processes, 14, 1981–1992, https://doi.org/10.1002/1099-1085(20000815/30)14:11/12<1981::AID-HYP49>3.0.CO;2-F, 2000.

Desai, S. D.: Observing the pole tide with satellite altimetry, Journal of Geophysical Research: Oceans, 107, 7–1–7–13, https://doi.org/10.1029/2001JC001224, 2002.

https://doi.org/10.5194/essd-2026-639
Preprint. Discussion started: 29 September 2026

Drob, D. P., Emmert, J. T., Meriwether, J. W., Makela, J. J., Doornbos, E., Conde, M., Hernandez, G., Noto, J., Zawdie, K. A., McDonald, S. E., Huba, J. D., and Klenzing, J. H.: An update to the Horizontal Wind Model (HWM): The quiet time thermosphere, Earth and Space Science, 2, 301–319, https://doi.org/10.1002/2014EA000089, 2015.

Ellmer, M.: Contributions to GRACE gravity field recovery: Improvements in dynamic orbit integration, stochastic modelling of the antenna offset correction, and co-estimation of satellite orientations, Ph.D. thesis, Graz University of Technology, ISBN 978-3-85125-646-8, https://doi.org/10.3217/n000g-efz85, 2018.

Ellmer, M. and Mayer-Gürr, T.: High precision dynamic orbit integration for spaceborne gravimetry in view of GRACE Follow-on, Advances in Space Research, 60, 1–13, https://doi.org/10.1016/j.asr.2017.04.015, 2017.

Etten, W. C. V.: Introduction to Random Signals and Noise, John Wiley & Sons, ISBN 9780470024126, 2006.

Featherstone, W. E., Brown, N. J., Mccubbine, J. C., and Filmer, M. S.: Description and release of Australian gravity field model testing data, Australian Journal of Earth Sciences, 65, 1–7, https://doi.org/10.1080/08120099.2018.1412353, 2018.

Floberghagen, R., Fehringer, M., Lamarre, D., Muzi, D., Frommknecht, B., Steiger, C., Piñeiro, J., and da Costa, A.: Mission design, operation and exploitation of the gravity field and steady-state ocean circulation explorer mission, Journal of Geodesy, 85, 749–758, https://doi.org/10.1007/s00190-011-0498-3, 2011.

Folkner, W. M.: Planetary ephemeris DE432, Tech. rep., Jet Propulsion Laboratory, California Institute of Technology, https://naif.jpl.nasa.gov/pub/naif/generic_kernels/spk/planets/de432.pdf, 2014.

Ghobadi-Far, K., Han, S. C., McCullough, C. M., Wiese, D. N., Yuan, D. N., Landerer, F. W., Sauber, J., and Watkins, M. M.: GRACE Follow-On Laser Ranging Interferometer Measurements Uniquely Distinguish Short-Wavelength Gravitational Perturbations, Geophysical Research Letters, 47, https://doi.org/10.1029/2020GL089445, 2020.

Goiginger, H., Rieser, D., Mayer-Gürr, T., Pail, R., Fecher, T., Gruber, T., Albertella, A., Maier, A., Höck, E., Krauss, S., Hausleitner, W., Baur, O., Jäggi, A., Meyer, U., Brockmann, J. M., Schuh, W.-D., Krasbutter, I., and Kusche, J.: The satellite-only global gravity field model GOCO02s, Presentation at the European Geosciences Union (EGU) General Assembly 2011, 2011.

Gruber, T., Visser, P. N., Ackermann, C., and Hosse, M.: Validation of GOCE gravity field models by means of orbit residuals and geoid comparisons, Journal of Geodesy, 85, 845–860, https://doi.org/10.1007/s00190-011-0486-7, 2011.

Hirt, C., Kuhn, M., Claessens, S., Pail, R., Seitz, K., and Gruber, T.: Study of the Earth's short-scale gravity field using the ERTM2160 gravity model, Computers & Geosciences, 73, 71–80, https://doi.org/10.1016/j.cageo.2014.09.001, 2014.

Ince, E. S., Barthelmes, F., Reißland, S., Elger, K., Förste, C., Flechtner, F., and Schuh, H.: ICGEM – 15 years of successful collection and distribution of global gravitational models, associated services, and future plans, Earth System Science Data, 11, 647–674, https://doi.org/10.5194/essd-11-647-2019, 2019.

Jensen, L., Dill, R., Balidakis, K., Grimaldi, S., Salamon, P., and Dobslaw, H.: Global 0.05° water storage simulations with the OS LISFLOOD hydrological model for geodetic applications, Geophysical Journal International, 241, 1839–1851, https://doi.org/10.1093/gji/ggaf129, 2025.

JPL: GRACE LEVEL 1B JPL RELEASE 3.0, NASA Physical Oceanography Distributed Active Archive Center [data set], https://doi.org/10.5067/GRJPL-L1B03, 2018.

JPL: GRACE-FO Level-1B Release version 4.0 from JPL in ASCII, NASA Physical Oceanography Distributed Active Archive Center [data set], https://doi.org/10.5067/GFL1B-ASJ04, 2019.

Khintchine, A.: Korrelationstheorie der stationären stochastischen Prozesse, Mathematische Annalen, 109, 604–615, https://doi.org/10.1007/BF01449156, 1934.

Knijff, J. M. V. D., Younis, J., and Roo, A. P. J. D.: LISFLOOD: a GIS-based distributed model for river basin scale water balance and flood simulation, International Journal of Geographical Information Science, 24, 189–212, https://doi.org/10.1080/13658810802549154, 2010.

Koch, K. R. and Kusche, J.: Regularization of geopotential determination from satellite data by variance components, Journal of Geodesy, 76, 259–268, https://doi.org/10.1007/s00190-002-0245-x, 2002.

Kvas, A. and Mayer-Gürr, T.: GRACE gravity field recovery with background model uncertainties, Journal of Geodesy, 93, https://doi.org/10.1007/s00190-019-01314-1, 2019.

Kvas, A., Behzadpour, S., Ellmer, M., Klinger, B., Strasser, S., Zehentner, N., and Mayer-Gürr, T.: ITSG-Grace2018: Overview and Evaluation of a New GRACE-Only Gravity Field Time Series, Journal of Geophysical Research: Solid Earth, 124, 9332–9344, https://doi.org/10.1029/2019JB017415, 2019.

Kvas, A., Brockmann, J. M., Krauss, S., Schubert, T., Gruber, T., Meyer, U., Mayer-Gürr, T., Schuh, W. D., Jäggi, A., and Pail, R.: GOCO06s-A satellite-only global gravity field model, Earth System Science Data, 13, https://doi.org/10.5194/essd-13-99-2021, 2021.

Landerer, F., Flechtner, F., Save, H., and Dahle, C.: GRACE Follow-On Science Data System Newsletter (No. 24), Tech. rep., NASA Jet Propulsion Laboratory (JPL), https://www.gfz.de/fileadmin/gfz/sec12/pdf/GRACE-FO/GRACE_FO_SDS_newsletter_No24.pdf, 2023.

Landerer, F. W., Flechtner, F. M., Save, H., Webb, F. H., Bandikova, T., Bertiger, W. I., Bettadpur, S. V., Byun, S. H., Dahle, C., Dobslaw, H., Fahnestock, E., Harvey, N., Kang, Z., Kruizinga, G. L., Loomis, B. D., McCullough, C., Murböck, M., Nagel, P., Paik, M., Pie, N., Poole, S., Strekalov, D., Tamisiea, M. E., Wang, F., Watkins, M. M., Wen, H. Y., Wiese, D. N., and Yuan, D. N.: Extending the Global Mass Change Data Record: GRACE Follow-On Instrument and Science Data Performance, Geophysical Research Letters, 47, https://doi.org/10.1029/2020GL088306, 2020.

Liang, W., Li, J., Xu, X., Zhang, S., and Zhao, Y.: A High-Resolution Earth's Gravity Field Model SGG-UGM-2 from GOCE, GRACE, Satellite Altimetry, and EGM2008, Engineering, 6, 860–878, https://doi.org/10.1016/j.eng.2020.05.008, 2020.

Lütkepohl, H.: Chapter 6: Vector autoregressive models, in: Handbook of Research Methods and Applications in Empirical Macroeconomics, Edward Elgar Publishing, ISBN 9780857931016, https://doi.org/10.4337/9780857931023.00012, 2013.

Mayer-Gürr, T.: Gravitationsfeldbestimmung aus der Analyse kurzer Bahnbögen am Beispiel der Satellitenmissionen CHAMP und GRACE, Ph.D. thesis, Institut für Theoretische Geodäsie der Universität Bonn, http://hss.ulb.uni-bonn.de/diss_online, 2006.

Mayer-Gürr, T., Rieser, D., Zehentner, N., Pail, R., Gruber, T., Fecher, T., Rexer, M., Schuh, W.-D., Kusche, J., Brockmann, J. M., Krasbutter, I., Becker, S., Eicker, A., Schall, J., Baur, O., Höck, E., Hausleitner, W., Maier, A., Krauss, S., Jäggi, A., Meyer, U., and Prange, L.: The new combined satellite only model GOCO03s, Presentation at the International Symposium on Gravity, Geoid and Height Systems (GGHS) 2012, 2012.

Mayer-Gürr, T., Pail, R., Gruber, T., Fecher, T., Rexer, M., Schuh, W.-D., Kusche, J., Brockmann, J. M., Rieser, D., Zehentner, N., Kvas, A., Klinger, B., Baur, O., Höck, E., Krauss, S., and Jäggi, A.: The combined satellite gravity field model GOCO05s, Presentation at the European Geosciences Union (EGU) General Assembly 2015, 2015.

Mayer-Gürr, T., Behzadpour, S., Eicker, A., Ellmer, M., Koch, B., Krauss, S., Pock, C., Rieser, D., Strasser, S., Süsser-Rechberger, B., Zehentner, N., and Kvas, A.: GROOPS: A software toolkit for gravity field recovery and GNSS processing, Computers and Geosciences, 155, https://doi.org/10.1016/j.cageo.2021.104864, 2021.

Moritz, H.: Geodetic reference system 1980, Bulletin géodésique, 54, 395–405, https://doi.org/10.1007/BF02521480, 1980.

Müller, L., Müller, V., and Misfeldt, M.: AEI LRI1B v54, Max-Planck Institute for Gravitational Physics (Albert Einstein Institut) [data set], https://www.aei.mpg.de/grace-fo-ranging-datasets, 2024.

Öhlinger, F., Mayer-Gürr, T., Krauß, S., Dumitraschkewitz, P., Süsser-Rechberger, B., Strasser, A., Tieber-Hubmann, C., and Brockmann, J. M.: The satellite-only gravity field model GOCO2025s, Graz University of Technology Repository [data set], https://doi.org/10.3217/f48p8-8h651, 2025.

Pail, R., Goiginger, H., Schuh, W. D., Hck, E., Brockmann, J. M., Fecher, T., Güruber, T., Mayer-Gürr, T., Kusche, J., Jäggi, A., and Rieser, D.: Combined satellite gravity field model GOCO01S derived from GOCE and GRACE, Geophysical Research Letters, 37, https://doi.org/10.1029/2010GL044906, 2010.

Pail, R., Bruinsma, S., Migliaccio, F., Förste, C., Goiginger, H., Schuh, W. D., Höck, E., Reguzzoni, M., Brockmann, J. M., Abrikosov, O., Veicherts, M., Fecher, T., Mayrhofer, R., Krasbutter, I., Sansò, F., and Tscherning, C. C.: First GOCE gravity field models derived by three different approaches, Journal of Geodesy, 85, 819–843, https://doi.org/10.1007/s00190-011-0467-x, 2011.

Pail, R., Yeh, H. C., Feng, W., Hauk, M., Purkhauser, A., Wang, C., Zhong, M., Shen, Y., Chen, Q., Luo, Z., Zhou, H., Liu, B., Zhao, Y., Zou, X., Xu, X., Zhong, B., Haagmans, R., and Xu, H.: Next-generation gravity missions: Sino-European numerical simulation comparison exercise, Remote Sensing, 11, https://doi.org/10.3390/rs11222654, 2019.

Pavlis, N. K., Holmes, S. A., Kenyon, S. C., and Factor, J. K.: The development and evaluation of the Earth Gravitational Model 2008 (EGM2008), Journal of Geophysical Research: Solid Earth, 117, https://doi.org/10.1029/2011JB008916, 2012.

Petit, G. and Luzum, B.: IERS conventions (2010), Verlag des Bundesamts für Kartographie und Geodäsie, 36, 180, https://iers-conventions.obspm.fr/content/tn36.pdf, 2010.

Rao, K. R. and Yip, P. C.: Discrete cosine transform : algorithms, advantages, applications, Academic Press, ISBN 9780125802031, 1990.

Ray, R. D.: Documentation for Goddard Ocean Tide Solution GOT5: Global Tides from Multi-mission Satellite Altimetry, Tech. rep., Goddard Space Flight Center, https://ntrs.nasa.gov/citations/20250002085, 2025.

Reigber, C., Schwintzer, P., and Lühr, P.: The CHAMP geopotential mission, Bolletino di Geofisica Teorica ed Applicata, 40, 285–289, https://gfzpublic.gfz.de/pubman/item/item_228435, 1999.

Rummel, R.: Height unification using GOCE, Journal of Geodetic Science, 2, 355–362, https://doi.org/10.2478/v10156-011-0047-2, 2012.

Sandwell, D. T., Müller, R. D., Smith, W. H., Garcia, E., and Francis, R.: New global marine gravity model from CryoSat-2 and Jason-1 reveals buried tectonic structure, Science, 346, 65–67, https://doi.org/10.1126/science.1258213, 2014.

Shihora, L., Balidakis, K., Dill, R., Dahle, C., Ghobadi-Far, K., Bonin, J., and Dobslaw, H.: Non-Tidal Background Modeling for Satellite Gravimetry Based on Operational ECWMF and ERA5 Reanalysis Data: AOD1B RL07, Journal of Geophysical Research: Solid Earth, 127, https://doi.org/10.1029/2022JB024360, 2022.

Shihora, L., Liu, Z., Balidakis, K., Wilms, J., Dahle, C., Flechtner, F., Dill, R., and Dobslaw, H.: Accounting for residual errors in atmosphere–ocean background models applied in satellite gravimetry, Journal of Geodesy, 98, https://doi.org/10.1007/s00190-024-01832-7, 2024.

Sulzbach, R., Balidakis, K., Dobslaw, H., and Thomas, M.: TiME22: Periodic Disturbances of the Terrestrial Gravity Potential Induced by Oceanic and Atmospheric Tides, GFZ Data Services [data set], https://doi.org/10.5880/nerograv.2022.006, 2022.

Süsser-Rechberger, B., Krauss, S., Strasser, S., and Mayer-Guerr, T.: Improved precise kinematic LEO orbits based on the raw observation approach, Advances in Space Research, 69, 3559–3570, https://doi.org/10.1016/j.asr.2022.03.014, 2022.

Süsser-Rechberger, B., Mayer-Guerr, T., Krauss, S., Tieber-Hubmann, C., Schneider, S., and Steindorfer, M.: Precise dynamic orbit determination based on SLR for geodetic and upper atmosphere applications, Advances in Space Research, https://doi.org/10.1016/j.asr.2026.05.046, 2026.

https://doi.org/10.5194/essd-2026-639
Preprint. Discussion started: 29 September 2026

Tapley, B. D., Bettadpur, S., Ries, J. C., Thompson, P. F., and Watkins, M. M.: GRACE Measurements of Mass Variability in the Earth System, Science, 305, 503–505, https://doi.org/10.1126/science.1099192, 2004.

Tapley, B. D., Watkins, M. M., Flechtner, F., Reigber, C., Bettadpur, S., Rodell, M., Sasgen, I., Famiglietti, J. S., Landerer, F. W., Chambers, D. P., Reager, J. T., Gardner, A. S., Save, H., Ivins, E. R., Swenson, S. C., Boening, C., Dahle, C., Wiese, D. N., Dobslaw, H., Tamisiea, M. E., and Velicogna, I.: Contributions of GRACE to understanding climate change, Nature Climate Change, 9, 358–369, https://doi.org/10.1038/s41558-019-0456-2, 2019.

Tongji: Tongji_GMMG2021S, International Centre for Global Earth Models (ICGEM) [data set], https://icgem.gfz.de/getmodel/gfc/f81966ed1ca42cd6c0d5c7b5733fab62f6c5136cace452f1f009474b3bd2c0a3/Tongji-GMMG2021S.gfc, 2021.

van Westrum, D., Ahlgren, K., Hirt, C., and Guillaume, S.: A Geoid Slope Validation Survey (2017) in the rugged terrain of Colorado, USA, Journal of Geodesy, 95, https://doi.org/10.1007/s00190-020-01463-8, 2021.

Wielicki, B. A., Barkstrom, B. R., Harrison, E. F., Lee, R. B., Smith, G. L., and Cooper, J. E.: Clouds and the Earth's Radiant Energy System (CERES): An Earth Observing System Experiment, Bulletin of the American Meteorological Society, 77, https://doi.org/10.1175/1520-0477(1996)077<0853:CATERE>2.0.CO;2, 1996.

Wöske, F., Kato, T., Rievers, B., and List, M.: GRACE accelerometer calibration by high precision non-gravitational force modeling, Advances in Space Research, 63, 1318–1335, https://doi.org/10.1016/j.asr.2018.10.025, 2019.

Zhao, Y., Li, J., Xu, X., and Su, Y.: WHU-SWPU-GOGR2022S: A combined gravity model of GOCE and GRACE, International Centre for Global Earth Models (ICGEM) [data set], https://doi.org/10.5880/icgem.2023.003, 2023.

Zingerle, P., Pail, R., Gruber, T., and Oikonomidou, X.: The experimental gravity field model XGM2019e, International Centre for Global Earth Models (ICGEM) [data set], https://doi.org/10.5880/ICGEM.2019.007, 2019.

Zingerle, P., Pail, R., Gruber, T., and Oikonomidou, X.: The combined global gravity field model XGM2019e, Journal of Geodesy, 94, https://doi.org/10.1007/s00190-020-01398-0, 2020.